Synthesis and sintering of 1D Al_2O_3@MWCNTS ceramic composite with excellent mechanical and electrical properties for advanced engineering applications

K. Chand [a,*], T. Mustafa [b], A. H. Shah [c]
[a] *Key Laboratory of In-Fiber Integrated Optics, College of Physics and Optoelectronic Engineering, Harbin Engineering University, Harbin 150001, China*
[b] *Department of Chemical Engineering, Balochistan University of Information Technology, Engineering, and Management Sciences (BUITEMS), Quetta, 87300, Pakistan*
[c] *Department of Textile Engineering, Balochistan University of Information Technology, Engineering and Management Sciences, Quetta, 87300, Pakistan*

A novel strategy was exploited to synthesize one-dimensional (1D) Al_2O_3 ceramic by using MWCNTs as a template. The prepared amorphous alumina [$Al(OH)_3$] was annealed at high temperatures to convert it into corundum Al_2O_3. Homogeneous dispersion of MWCNTs was obtained by the deposition of Al_2O_3 on the MWCNTs surface. Then, the calcined 1D Al_2O_3@MWCNTs hybrid powder was sintered at 70 MPa and 1300 ˚C for 10 min using spark plasma sintering (SPS). The microstructure analysis confirmed the uniform distribution of MWCNTs in Al_2O_3 ceramic. The compressive residual stresses on MWCNTs lead to a much stronger grain boundary as well as higher interfacial shear strength between the outer wall of MWCNT and Al_2O_3 ceramic. As a result, by the addition of only ~1.27 wt.% MWCNTs, the flexural strength and fracture toughness along with higher electrical conductivity (315 S/m) were simultaneously enhanced up to ~70% and ~73%, respectively, with respect to monolithic Al_2O_3.

(Received May 2, 2024; Accepted July 2, 2024)

Keywords: Alumina, Carbon nanotubes, Ceramic composites, Spark plasma sintering, Mechanical enhancement

1. Introduction

Nowadays, the advanced applications of conventional ceramics require higher performances and functions, which are difficult to achieve with monolithic ceramics. Therefore, many developments have been made by engineering microstructure or reinforcement of second-phase fillers such as nanosheets, nanotubes, or nanoparticles in a matrix to improve their properties [1, 2]. Advanced ceramics such as Al_2O_3, TiO_2 TiC, SiC, SiN_3, etc., have distended properties like mechanical (strength, hardness, toughness, and elastic modulus), chemical, and stability in harsh environments attribute the ceramics superior to metals and polymers [3-6]. Among these, Al_2O_3 is an imperative engineering ceramic extensively used in cutting tools, energy transportation, aerospace, military, chemical industry, and so on. Regardless of these excellent properties, Al_2O_3 has limited use in advanced structural applications because of its brittleness, which is due to combined ionic and covalent bonds [7].

It is also possible to increase the fracture toughness of ceramic at the expense of strength [8, 9]. This is the biggest challenge when developing the structural ceramic to increase the toughness as well as the strength. In the recent past, carbon based materials such as carbon nanotubes, graphene, graphene oxide, etc have paved way for the researchers to develop a composite with the ceramics due to its enhanced mechanical, electrical and thermal properties. Carbon nanotube is used as the reinforcement material in ceramic matrix composites because of reasons such as chemical inertness, wear resistance, high aspect ratio and low density. But it has been shown that the ability

* Corresponding authors: kishor.vallasai@hrbeu.edu.cn
https://doi.org/10.15251/DJNB.2024.193.1021

of CNTs to reinforce the ceramic matrix is not as good (due to the agglomeration of CNTs) even though the CNTs have very high mechanical strength [10-12]. Therefore, the strengthening or the toughening effect is strongly dependent on the load transfer between the ceramic matrix and the CNTs or vice versa and the distribution of the CNTs. Therefore, various approaches have been employed to enhance dispersion CNTs into a ceramic matrix composite [8, 10, 13-16]. However, the particle size and dimension of the Al_2O_3 powder are also found to be very significant in determining the properties of the Al_2O_3 composites [13, 15-18].

So far, several methods have been used to fabricate CNTs incorporated in Al_2O_3 ceramic composites. For instance, M. Estili et al. [18] used surfactantless modified MWCNTs to get homogeneous dispersion in α-Al_2O_3 nanoparticles by using simple powder technology. After consolidation by SPS, load-carrying and reinforcing capabilities were investigated in MWCNTs/Al_2O_3 ceramic composite. Uniformly incorporated MWCNTs significantly enhance the fracture energy by crack deflection and pullout of MWCNTs from ceramics. A. L. Myz et al. [13] reported that Al_2O_3 nanoparticles could mix with MWCNTs by ball milling, followed by SPS. Fabricated MWCNTs/Al_2O_3 composite showed higher electrical conductivity, which may have many applications in wireless communications, electronics, and nuclear physics. Evers, K. et al. [8] fabricated MWCNTs coated Al_2O_3 micro-platelets by using chemical vapor deposition (CVD). They used CVD for the in-situ growth of MWCNT on the surface of alumina platelets to get the nacre-like structure of the MWCNT/Al_2O_3 composite. Toughness was calculated in terms of work of fracture (47-106 J/m^2), which is higher than that of monolithic (11- 47 J/m^2); however, flexural strength was reduced in the composite as compared to monolithic Al_2O_3. In our previous work [16], strengthening and toughening effects in MWCNTs/Al_2O_3 composite were evaluated. Al_2O_3 nanoplates were used as raw materials, which persuaded the orientation of MWCNTs in a composite after sintering, attributing the high energy dissipation, bridging, and pullout of MWCNTs, inducing the very effective load transfer.

In this research work, a general and simple strategy (colloidal processing) was applied to synthesize rod-like $Al(OH)_3$@MWCNTs hybrid powder by using MWCNTs as a template. In-situ growth of amorphous phase alumina (AA) on the surface of MWCNTs was converted into α-Al_2O_3 after heating at 1100 ˚C in Ar atmosphere. Mechanical and electrical properties and microstructure of homogeneously MWCNTs distributed Al_2O_3 composite were evaluated after consolidation at 70 MPa and 1300 ˚C.

2. Materials and methods

2.1. Raw materials

MWCNTs (graphitized, > 99 % purity, outer diameter 30-80 nm, length ≤ 10μm) powder was obtained from Aladdin Co. Ltd. Formic acid (≥98 %) and Aluminum sulfate octa-decahydrate ($Al_2(SO_4)_3$. $18H_2O$, ≥ 99. The reagents used in this study were purchased as follows: potassium hydroxide (KOH, ≥ 85. 99 %) and ammonium formate (CH_5NO_2, ≥ 99. 99 %) metal basis were obtained from Sinopharm Chemical Reagent Co. , Ltd. The commercial TM-DAR α-alumina (Al_2O_3) powder (~99. sp. gr. 2. 65, and 7 m^2/g specific surface area as per the company's information.

2.2. Synthesis of Al_2O_3@MWCNTs nanowires

MWCNTs were modified by acid treatment, as reported previously [16, 18]. 0.6 gm pristine MWCNTs was mixed with 100 ml of concentrated H_2SO_4 (98%) and 68% HNO_3 (3:1 v/v). The mixture was refluxed 100 - 120 ˚C for 10 - 20 min. Then, the refluxed mixture was diluted with distilled water and rinsed to obtain the constant pH by using a 0.2 μm PTFE membrane. The pure acid-treated MWCNTs were obtained after drying the cake in the oven at 90 ˚C in an oven. The pH of the solution was maintained using the formic acid-ammonium formate buffer solution, as reported previously [19]. Aluminum sulfate octa-decahydrate and MWCNTs were separately mixed in the prepared buffer solution. The ultrasonication (30 min) was used to mix the MWCNTs in a solution. As shown in Fig. 1, the MWCNTs solution was put in a beaker and increased the temperature during stirring. Aluminum sulfate octa-decahydrate solution was put drop wise (10

ml/min) method when the temperature reached up to 70 ˚C. Then, maintain the temperature of the solution at 70 ˚C for 2.5 hrs. Afterward, the reaction was completed by increasing the temperature up to 100 ˚C for a further 2.5 hrs. The remnant salts were removed by vacuum filtration and prepared $Al(OH)_3$@MWCNTs were dried in a freeze dryer for 36 hrs. Different mass ratios (MWCNT: Aluminum sulfate octa-decahydrate) were used to prepare different samples and given the name S-C1 (1:160), S-C2 (1:120), S-C3 (1:90) to control the concentration of MWCNTs in composites. Next, the prepared amorphous phase of $Al(OH)_3$@MWCNTs was converted into α phase Al_2O_3@MWCNTs after heating at 1100 ˚C in an Ar atmosphere using a tube furnace.

2.3. Fabrication of Al_2O_3/MWCNTs ceramic composite

Al_2O_3@MWCNTs hybrid powder was consolidated through pressure-assisted sintering. Spark plasma sintering (SPS) was carried out using Dr. sinter apparatus (SPS, Syntex Inc., Kanagawa, Japan). The specimens were sintered at 1300 ˚C with uniaxial pressure 70 MPa. The heating rate and dwell time were maintained at 100 ˚C/min and 10 min, respectively. After sintering, pressure was removed, and samples were cooled up to room temperature. The samples were removed from the sintering chamber and polished after removing the carbon sheets. The bulk densities of different polished specimens were determined using Archimede's method, and the theoretical densities of the specimens were calculated by following the rules of the mixture. The densities of Al_2O_3 and MWCNTs were assumed to be 3.98 g/cm^3 and 2.1 g/cm^3 respectively. The contents of MWCNTs were determined by heating the bulk composites in the air at 1300 ˚C for 24 hours to remove the complete MWCNTs from the composites. The results show the composition of MWCNTs as ~0.43 wt%, ~1.27 wt%, and ~1.78 wt% and given the names S-C1, S-C2, and S-C3 respectively.

2.4. Characterization techniques

The microstructure of the powder and bulk materials synthesized in this work was characterized using a Field Emission gun scanning electron microscope (FESEM instrument Jeol make model no, JSM-6700F). Then, the phase state of samples were analysed with the x-ray diffraction analysis instrument by using the D/Max-2550VB+/PC type machinery imported from Japan. Clearing and improving on the structure of the MWCNTs was achieved through Raman Spectroscopy Machine; inVia-reflex, Reninshaw from England. The specimens laser at 532 nm were used for analysis of the specimens provided at the range 100 to 4000 cm^{-1}. More so the microstructure at atomic level look of the samples was studied by following high resolution transmission electron microscope made from Japan (JEOL, Model no 200CX).

2.5. Mechanical and electrical properties measurements

The Young's modulus and Poisson's ratios were measured using advanced ultrasonic materials characterization equipment (UMS-100 France). The Anstis equation was used to calculate the fracture toughness.

$$K_{IC} = 0.016\left(E/H_v\right)^{0.5} PC^{-1.5} \quad (1)$$

where E = Young's modulus, P = the load, H = indentation hardness, and C = the length of half-crack. The indentation method was used to determine the Vicker's hardness at 49 N loads for 10 seconds.

A three-point bending technique was used for flexural strength (σ_f) measurements, with the specimen size 21(length) x 2 (width) x 2.5 (height). The loading speed and bending span for the flexural testing were 0.5 mm/min and 16 mm, respectively.

The electrical conductivity of the sintered specimen was measured using a Keithley 580 digital micro-ohmmeter, applying the two-point method to the silver electrode specimen.

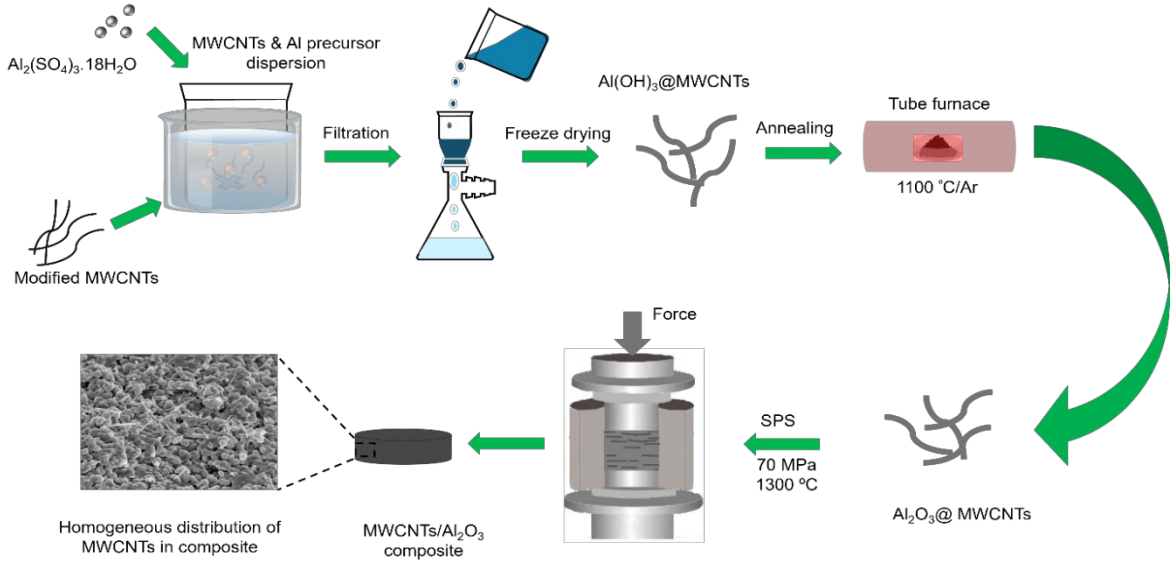

Fig. 1. Schematic diagram for the preparation of MWCNTs/Al_2O_3 composite, reproduced from [16].

3. Results and discussion

3.1. Preparation of controlled structure of Al_2O_3@MWCNTs composite

FESEM and TEM were used to characterize the morphology of acid-treated MWCNTs. Amorphous carbon was removed (Fig. 2a) after modification, and as shown in Fig. 2b, the outer diameter of MWCNT (48.7 ± 6 nm) was determined using image J software. The surface of MWCNTs has factionalized after the deposition of various functional groups, such as hydroxyl (-OH) and carboxyl (-COOH), which changed the properties of hydrophobic MWCNTs to hydrophilic ones. Some minor amounts of nano-defects produced during acid treatment are shown in the inset of Fig. 2b; however, the lattice structure remained the same as pristine MWCNT [20]. Due to hydrophilic properties, modified MWCNTs were easily dispersed in water and buffer solution. Next, sonication and thermal reaction decomposed the $Al_2(SO_4)_3.18H_2O$ into Al^+ and SO_4^- ions. After decomposition, Al^+ was embedded on the surface of functionalized MWCNTs. The core and shell structured $Al(OH)_3$@MWCNTs hybrid nanofibers were prepared after the deposition of amorphous $Al(OH)_3$ on the surface of MWCNTs. It is imperative to prevent the agglomeration of MWCNTs during the reaction; therefore, the pH of the solution was maintained between 4.4 and 4.5 for the first two hours. The Ultrathin film of AA was placed on the MWCNT surface at a comparatively lower temperature (70 ˚C). Then, the solution's temperature was increased up to 100 ˚C, enhancing the thermal decomposition of aluminum sulfate, which enhanced the concentration of Al^+ [21]. Positively charged Al^+ are nucleated on negatively charged MWCNT surface due to electrostatic attraction and increased thickness of the alumina layer. The controlled flow rate (drop by drop) of aluminum sulfate solution and the hydrolysis and adsorption rate of Al^+ in the solution were effectively controlled by maintaining pH at high temperatures. The deposited AA was converted into stable oxides of alumina by oxidation processes where Al^+ reacted with functional groups on the MWCNT surface to chemical bond by using different thermodynamics processes, which could be explained in the following equations [22, 23]:

$$Al^{3+} + 3(OH^-) \rightarrow Al(OH)_3, \quad \Delta H = 61.3\ KJ/mol \ \text{at}\ 273\ K \tag{2}$$

$$Al(OH)_3 \xrightarrow{\Delta} 1/2\, Al_2O_3 + 3/2\, H_2O, \quad \Delta H = 101.89\ KJ/mol \tag{3}$$

$$a - Al_2O_3 \xrightarrow{\Delta} \gamma - Al_2O_3 \xrightarrow{\Delta} \alpha - Al_2O_3 \tag{4}$$

$Al(OH)_3$@MWCNTs were successfully converted into α-Al_2O_3@MWCNTs without burning carbon nanotubes at high temperatures in an inert atmosphere. As shown in Fig. 2c, all MWCNTs are covered by Al_2O_3 to form core and shell structures. To the best of our knowledge, this is the first time that MWCNTs are used as a template to fabricate1D α-Al_2O_3 nanofibers. A smooth and controlled surface (Fig. 2d) confirms the structure stability of α-Al_2O_3@MWCNTs at high temperatures.

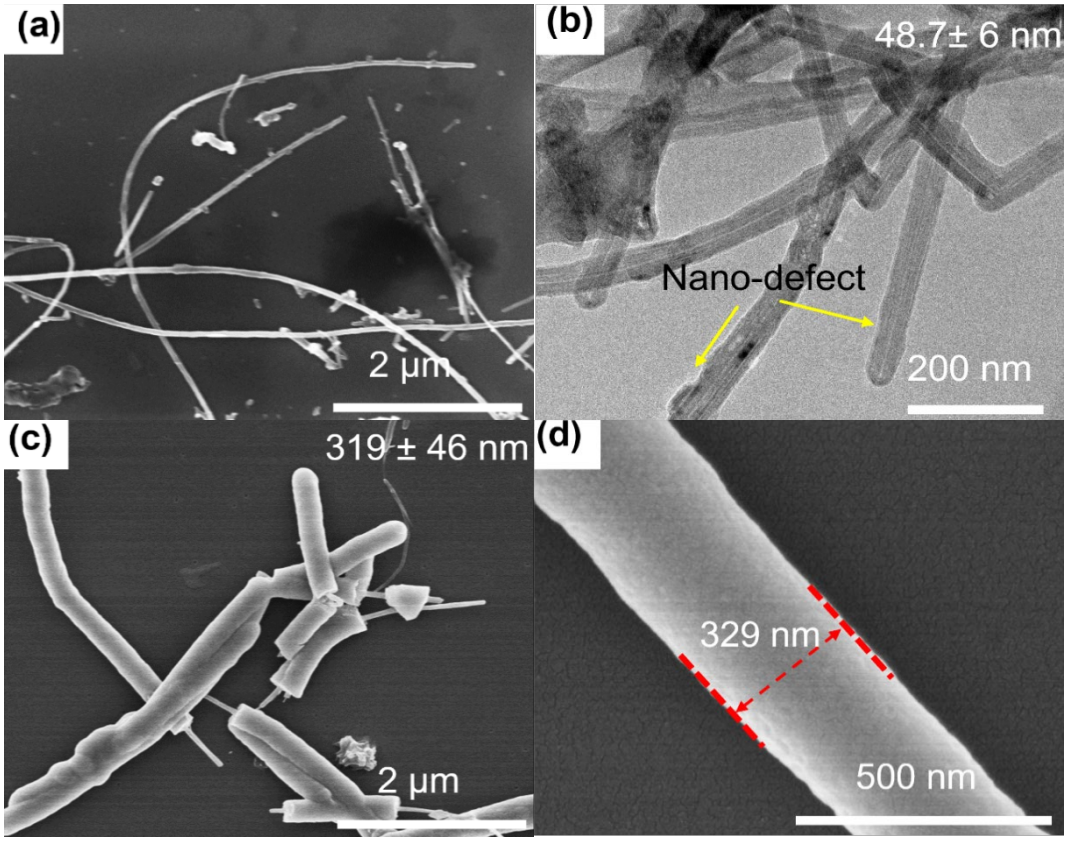

Fig. 2. (a) SEM of acid-treated MWCNTs, (b) TEM of MWCNTs, (c) SEM of Al_2O_3@MWCNTs, (d) Thickness of Al_2O_3@MWCNTs shown at higher magnification.

3.2. Phase constituents of 1D Al_2O_3/MWCNTs composites

Unstable AA oxidized the MWCNT during sintering, and we could not find MWCNT anymore due to the unstable amorphous powder of alumina. Therefore, the powder was heated in an Ar atmosphere at 1100 ˚C for 2.5 hrs to get a stable form of Al_2O_3 before sintering at high temperatures. XRD was used to evaluate the phase transformation and crystallization of Al_2O_3 that occurred by the nucleation of ions and electrons at different temperatures [21]. As shown in Fig. 3a, the sharp peak at lattice planes (002) confirms the highly ordered crystalline graphite in modified MWCNTs. The existence of (002) lattice plane suggests that hydrophilic and surfactant-less MWCNTs can be prepared with a crystalline structure similar to that of pristine MWCNTs. AA powder was annealed at 1100 ˚C, where it was completely converted into corundum α-phase. The stable α-Al_2O_3 maintained its corundum structure after sintering at high temperature (PDF# 46-1212). The crystalline structure of particles in Al_2O_3 ceramic induced higher mechanical properties. Therefore, the hexagonal closed pack (PDF# 46-1212) structure of corundum Al_2O_3 enhanced the strengthening effect in Al_2O_3/MWCNTs composites after sintering. However, we cannot observe the (002) peak related to MWCNTs in Al_2O_3/MWCNTs composites due to the limitation of XRD equipment and higher crystallinity of Al_2O_3 in a composite [16, 24, 25].

Raman spectroscopy has been used as a powerful tool to trace the MWCNTs (even a very small amount) in a composite. The defect mode (D-band) and graphite mode (G-band), in Raman

spectra, are the most important features which can be observed at about ~1350 cm^{-1} and ~1385 cm^{-1}, respectively [18]. The defect density of MWCNT depends on the intensity ratio (I_D/I_G); higher I_D/I_G confirms the higher quality of MWCNTs. Some defects could appear on the surface of MWCNTs, lowering the quality after acid treatment [10]. As indicated in Fig. 3b, the I_D/I_G of pure MWCNTs is 0.86 after acid treatment and 0.84 in $Al(OH)_3$@MWCNTs composites, and it is decreased up to 0.80 in Al_2O_3@MWCNTs powder after annealing at 1100 ˚C. However, sp^2 bonds visibly recovered (I_D/I_G = 0.67) in Al_2O_3/MWCNTs composite after sintering at high temperature. Moreover, the 2D band is very sensitive to phonon structure perturbation and represents the second-order two-phonon process in sp^2 carbon materials. The 2D band is used to determine the distortion of MWCNT in the ceramic composites. The shift of the 2D-band to forward or backward in Raman spectra indicates the weather compressive or tensile strain of MWCNTs, respectively. As shown in Fig. 3c, the 2D-band is shifted backward (2657 cm^{-1}) in $Al(OH)_3$@MWCNTs and (2671 cm^{-1}) in Al_2O_3/MWCNTs powder after annealing, as compared to pure MWCNTs (2695 cm^{-1}) showing the tensile strain. However, the 2D-band shifted to 2701 cm^{-1} in the Al_2O_3/MWCNTs composite after sintering from 2695 cm^{-1}, indicating that compressive strain was applied to MWCNTs in the ceramic composite. These residual stresses were produced by chemical treatment, heat treatment, mechanical, and other joined processes, etc. They could "interlock" the component in a composite in the absence of external load.

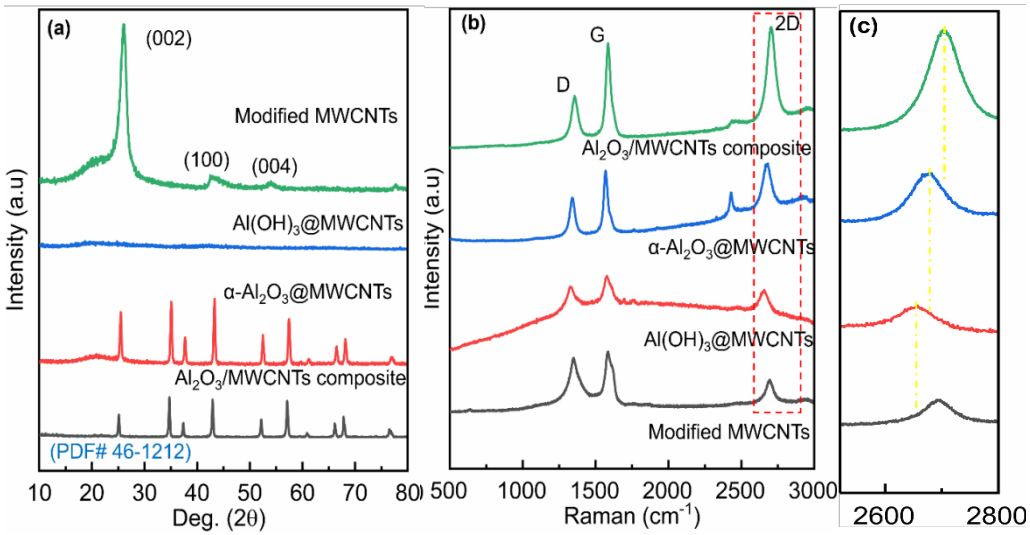

Fig. 3. Powder characterization: (a) X-ray diffraction, (b) Raman spectra of pure MWCNTs, amorphous phase of composite, Al_2O_3@MWCNTs hybrid powder after annealing at 1100 ˚C, and Al_2O_3/MWCNTs sintered composite, and (c) Representation of enlarged 2D peak in b.

3.3. Microstructure and properties evaluation of 1D Al_2O_3/MWCNTs composite

The microstructure, filler distribution, and density are critical parameters that affect the mechanical and functional properties of ceramic composites. Higher relative densities **(Table 1)** of bulk materials revealed good consolidation during SPS. The SPS is very helpful in arranging the micro-structure of the Al_2O_3/MWCNTs composite. The densities of composites were determined by Archimedes' principles and calculated by the rule of mixtures. Agglomeration of second-phase filler in a ceramic matrix can effectively deteriorate the mechanical strength and toughness. Therefore, this novel strategy (core and shell structure formation) was applied to prevent the cluster formation of MWCNTs in Al_2O_3 composites. The MWCNTs covered by Al_2O_3 were compressed between Al_2O_3 ceramic grains after hot pressing by SPS.

Table 1. Physical properties of specimens.

Sample	Poisson's Ratio	Rule of mixtures density (g/cm^3)	Obtained density (g/cm^3)	Relative density (%)
S-C0	0.26 ± 0.01	3.987	3.98 ± 0.03	99.9
S-C1	0.25 ± 0.01	3.98	3.948 ± 0.02	99.2
S-C2	0.24 ± 0.02	3.963	3.93 ± 0.03	99.1
S-C3	0.23 ± 0.01	3.953	3.86 ± 0.05	97.5

Mechanical properties and electrical conductivity of monolithic Al_2O_3 and composites with different concentrations of MWCNTs are explained in Fig. 4. MWCNTs controlled the growth of grains (small grain size improved the mechanical properties) of the ceramic matrix during sintering. It has caused the strength enhancement of composite [26]. Young's modulus was measured as the intrinsic mechanical property of a material, which could be determined from the elastic properties of the components in the ceramic composites. As shown in Fig. 4a, Young's modulus is decreased from 403.19 ± 6.9 to 381.11 ± 9.3 GPa with increasing the concentration of MWCNTs up to ~1.78 wt.% in composites, which is consistent as reported previously [10, 16, 19]. Grain size and hardness are reliable with each other, and smaller grain sizes could lead to higher values of hardness in ceramic composites. However, it has been reported that hardness decreased with increasing the concentration of second-phase filler [16, 27, 28]. The hardness of samples S-C1 increased from 19.1 ± 0.38 to 19.8 ± 0.43 GPa and is higher than that of monolithic Al_2O_3 ceramic (Fig. 4a). However, hardness decreased by further increasing the concentration of MWCNTs. Hence, the SPS consolidated MWCNTs matrix with ~1.27 wt.% of MWCNTs has optimum mechanical properties with 99.1% relative density. The bending strength and indentation fracture toughness (Fig. 4b) of the S-C2 were 669.43 ± 33.6 MPa (~ 70% increased as compared to monolithic alumina), 6.35 ± 0.29 $MPa.m^{1/2}$ (~ 73% increased as compared to monolithic alumina), respectively.

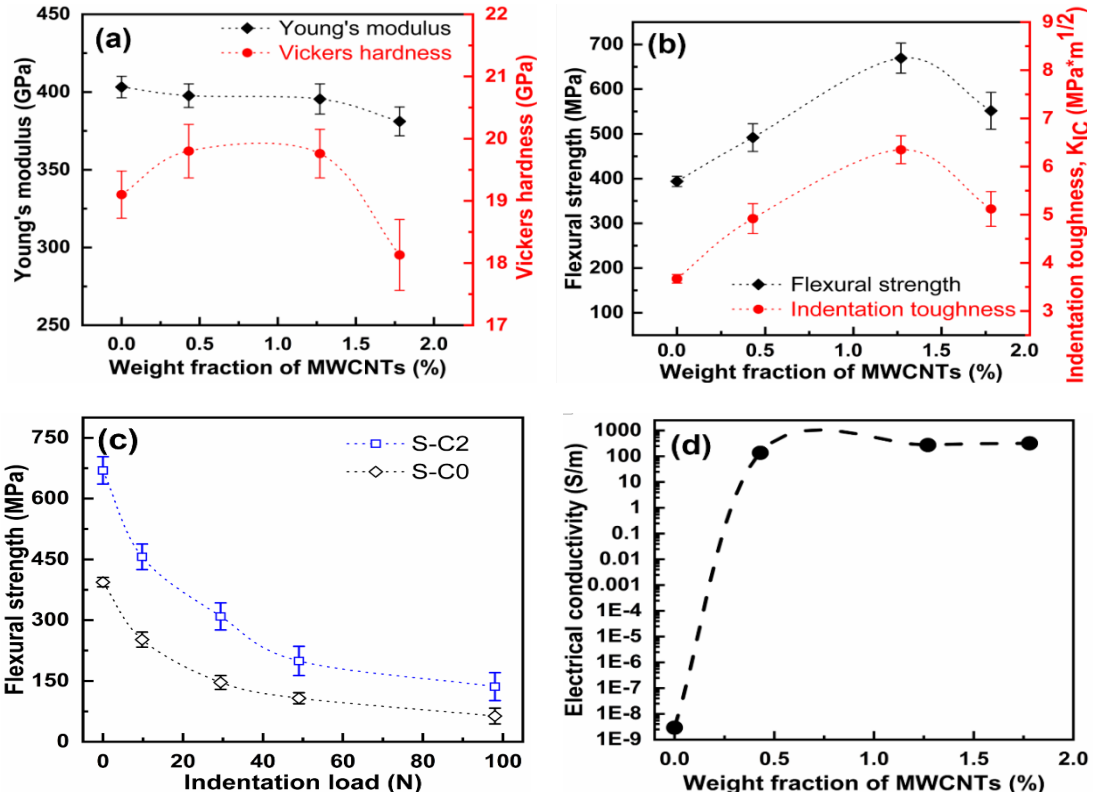

Fig. 3. Evaluation of Young's modulus and Vickers hardness (a), Flexural strength, and Indentation toughness (b) by increasing the concentration of MWCNTs in composites, Flexural strength after applying indentation load for monolithic Al_2O_3 and Al_2O_3/composite (c), Electrical conductivity for composites with increasing MWCNTs contents (d).

The flexural strength and fracture toughness show a similar trend, inducing the positive effect of indentation fracture toughness on the strength. The toughening mechanism effect of MWCNTs in ceramic matrices has been reported in several studies [8, 29]. However, it is rare to simultaneously achieve such high strength and toughness. Furthermore, the monolithic Al_2O_3 and 1D Al_2O_3/MWCNTs composite showed lower flexural strength after indentation load. However, as shown in Fig. 4c, higher strength in Al_2O_3/MWCNTs composite induced the higher damage tolerance of MWCNTs reinforced ceramic matrix. It has also been observed that bending strength diminished slowly by increasing the indentation load, suggesting the existence of fracture resistance in composites. Moreover, the electrical conductivity was increased by the addition of MWCNT contents. As shown in Fig. 4d, electrical conductivity showed a maximum value of around ~191 S/m after the addition of only 0.43 wt.% MWCNTs. It further increased by the addition of more MWCNTs (~1.27 wt.% and ~1.78 wt.%) contents up to ~315 S/m and ~320 S/m, respectively.

Subsequently, the polished surface and microstructure of Al_2O_3/MWCNTs composite were investigated through FESEM (Fig. 5). The grain boundary strength, grain size, and relative density of the ceramic composites critically influence the flexural strength and toughness. The second phase filler impeded the grain growth during sintering. Fig. 5a showed the smaller grain size (360 ± 148 nm) in Al_2O_3/MWCNTs composite where the homogeneous distribution of MWCNTs effectively hindered the grain growth as compared to monolithic Al_2O_3 nanoparticles [21]. In addition, the thermally etched polish surface shows very limited pores at triple junctions, which induces grain growth along MWCNTs. Besides, the fracture surface confirms the homogeneous distribution of MWCNTs in the Al_2O_3 matrix. As shown in Fig. 5b, MWCNTs were protruded on the fracture surface and homogeneously distributed without any agglomeration. After sintering, the highly preserved structure of protruded MWCNT has been recognized on the fracture surface under SEM observation (Fig. 5c). Sword-and-sheath fracture of MWCNT can be easily seen on the fracture surface and shown by the yellow circle in Fig. 5c revealing the pullout behavior. Such pullout behavior is ascribed to the toughening enhancement of composite. Additionally, transgranular fracture (Fig. 5d) attributes the much stronger grain boundary, inducing the higher strengthening effect in the Al_2O_3/MWCNTs composite.

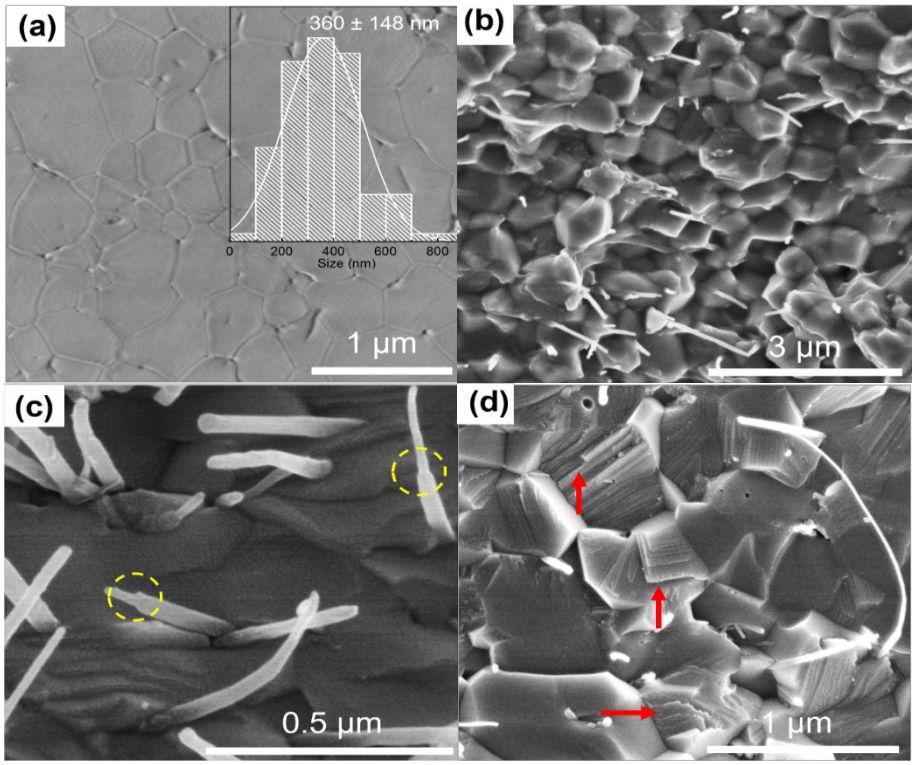

Fig. 4. (a) SEM of thermally etched surface Al_2O_3/MWCNTs composites for grain size measurement, the grain size distribution are shown in the inset, (b) Fracture surface of Al_2O_3/MWCNTs composite, (c) Sword and sheet fracture MWCNTs in composite is shown by yellow circle, (d) Trans-granular fracture behavior of Al_2O_3/MWCNTs composite.

Usually, intergranular fracture is exhibited in a monolithic Al_2O_3 ceramic matrix. The conversion of fracture behavior from intergranular to transgranular reflected the microstructure changes by the addition of MWCNTs. Therefore, STEM and TEM were exploited to disclose the exceptional microstructure of the Al_2O_3/MWCNTs composite. As shown in Fig. 6a, a large number of MWNCTs were aligned inside the grains instead of long grain boundaries. The alignment of MWCNTs in such a way has been rarely observed in the MWCNTs-reinforced ceramic composites [1, 30]. Furthermore, TEM-EDS mapping was used to reveal the concentration of C, Al, and O, confirming the existence of MWCNTs in composite. Although a smaller grain size induces the intergranular fracture, the embedded MWCNTs through two or more Al_2O_3 grains like a needle significantly improve the strength of grain boundaries to attribute the transgranular fracture. Besides, compressive stresses also have significantly improved the fatigue life of composite [31]. It has been observed that the hollow core for most of the MWCNTs in the composite disappeared (Fig. 6b). Besides, forward-shifted 2D peak in Raman spectra (Fig. 3c) of MWCNT/ceramic composite also indicated the compressive stresses after sintering [32, 33]. Compressive residual stresses in MWCNT/ceramic composite are often generated during SPS at high temperatures by the mismatch of coefficients of thermal expansion (CTE) between the MWCNTs and ceramic matrix [34, 35]. These stresses in MWCNTs/ceramic matrix helped reduce the diameter of MWCNTs after the fabrication of the composite, which revealed the densification of MWCNTs during sintering. Then, it indicated the rough surface of MWCNT and strong interfacial interaction. It enhanced the load transfer efficiency from the alumina matrix to MWCNTs. In addition, compressive residual stresses of MWCNTs exploited the strong inter-wall shear resistance (ISR) that attributed the load transfer not only by MWCNT's outermost walls but also into the inner walls. It has improved the mechanical responses of ceramic matrix [34, 36]. Nano-defects (Fig. 2b) were completely wetted with ceramic matrix, which mechanically interlocked the outermost wall of MWCNTs with ceramic matrix and improved the ISR [37, 38]. Because of good wetting, acid-treated MWCNTs were uniformly compressed in a ceramic matrix, which provided uniform and excellent compressive stress throughout the MWCNTs structure.

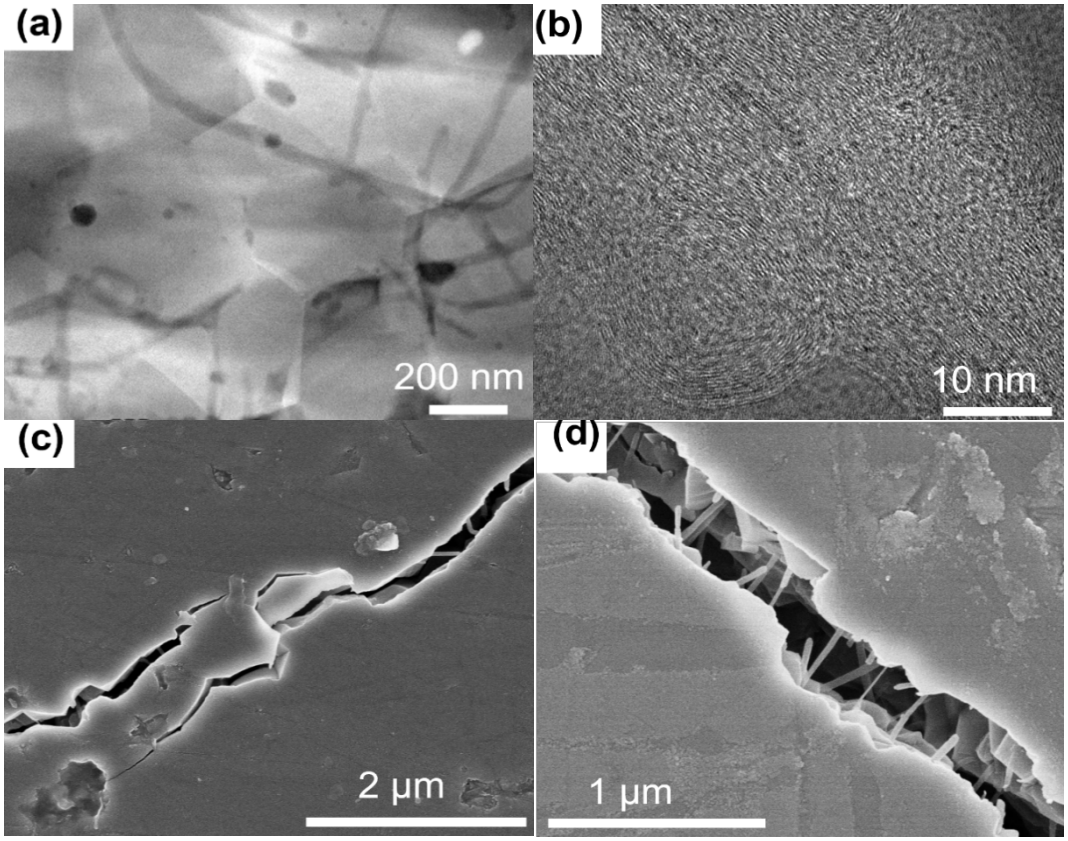

Fig. 5. STEM observation confirms the presence of MWCNTs in Al_2O_3@MWCNTs composites, (b) HRTEM showed compression of MWCNTs without hollow in a composite, (c) SEM of crack propagation of Al_2O_3/MWCNTs composite to trans-granular behavior, (d) Crack bridging by MWCNTs at higher magnification.

The toughening mechanisms of MWCNTs reinforced ceramic matrix were investigated by SEM observation of crack propagation (deflection, crack bridging, and pullout) after indentation of the polished surface. Fig. 6c-d illustrates the toughening mechanisms of MWCNTs, where the toughening effect depends to a large extent on the boundaries between the MWCNTs and the matrix face connection conditions. MWCNTs can withstand 40% of the strain before breaking [39]. Intimate interfacial contact of uniformly distributed MWCNTs (which exist in the crack path having suitable length) with Al_2O_3 ceramic affected the crack propagation [18, 40]. As shown in Fig. 6c, a large number of deflection and branches have been observed deducing the fracture energy dissipation.

4. Conclusion

The novel strategy was successfully applied to deposited Al_2O_3 on 1D MWCNT for complete dispersion of MWCNTs in the Al_2O_3 matrix. Acid-treated MWCNTs were used to attract Al^+ and synthesize 1D Al_2O_3 on the surface of MWCNTs. Amorphous alumina hydroxide was converted into stable α-Al_2O_3 after annealing at 1100 ˚C in an argon atmosphere. MWCNTs inside the Al_2O_3 were completely preserved after heating at high temperatures, which can be easily observed by SEM investigation. Therefore, this new strategy opens the gateway to fabricate a controlled structure of 1D ceramic materials by using MWCNTs as a template. Furthermore, the Al_2O_3/MWCNTs composite was fabricated via SPS from the prepared Al_2O_3@MWCNTs hybrid powder by the addition of only ~1.27 wt.% MWCNTs in Al_2O_3 matrix, we obtained electrically conductive, mechanically strong, and tough Al_2O_3/MWCNTs composite. The transgranular fracture mechanism improved the grain boundary strength to enhance the flexural strength. Crack bridging and MWCNT pullout enhanced the fracture toughness in the composite. Such marvelous results were obtained from reduced grain size and uniform microstructure obtained from this study.

References

[1] S. Manafi, M. Ebrahimi, F. S. Bidabadi, I. Mobasherpour, Ceramics International, 2019, 45, 15928-15933; https://doi.org/10.1016/j.ceramint.2019.05.101

[2] J. Wozniak, A. Jastrzębska, T. Cygan, A. Olszyna, J. Eur. Ceram. Soc., 2017, 37, 1587-1592; https://doi.org/10.1016/j.jeurceramsoc.2016.11.010

[3] J. Liu, H. Yan, K. Jiang, Ceramics International, 2013, 39, 6215-6221; https://doi.org/10.1016/j.ceramint.2013.01.041

[4] I. Ahmad, H. Cao, H. Chen, H. Zhao, A. Kennedy, Y. Q. Zhu, Journal of the European Ceramic Society, 2010, 30, 865-873; https://doi.org/10.1016/j.jeurceramsoc.2009.09.032

[5] M. Ipek, S. Zeytin, C. Bindal, Journal of Alloys and Compounds, 2011, 509, 486-489; https://doi.org/10.1016/j.jallcom.2010.09.073

[6] V. Rajendar, T. Sowmya, K. V. Rao, B. Poornaprakash, M. Kumar, S. H. Park, Digest Journal of Nanomaterials and Biostructures, 2016, 11, 1083-1089.

[7] T. Cygan, J. Wozniak, M. Kostecki, M. Petrus, A. Jastrzebska, W. Ziemkowska,A. Olszyna, Ceram. Int., 2017, 43, 6180-6186; https://doi.org/10.1016/j.ceramint.2017.02.015

[8] K. Evers, H. Porwal, R. I. Todd, N. Grobert, Carbon, 2019, 145, 586-595; https://doi.org/10.1016/j.carbon.2019.01.060

[9] M. E. Launey, R. O. Ritchie, Adv. Mater., 2009, 21, 2103-2110; https://doi.org/10.1002/adma.200803322

[10] Y. C. Fan, E. H. Song, T. Mustafa, R. C. Liu, P. P. Qiu, W. W. Zhou, Z. X. Zhou, A. Kawasaki, K. Shirasu, T. Hashida, J. J. Liu, L. J. Wang, W. Jiang, W. Luo, Adv. Sci., 2020, 7, 9.

[11] M.-F. Yu, O. Lourie, M. J. Dyer, K. Moloni, T. F. Kelly, R. S. Ruoff, Science, 2000, 287, 637-640; https://doi.org/10.1126/science.287.5453.637

[12] M. Murarescu, D. Dima, G. Andrei, A. Circiumaru, Digest Journal of Nanomaterials and Biostructures, 2014, 9, 653 - 665.

[13] A. L. Myz, O. V. Kichai, G. R. Karagedov, R. A. Shutilov, V. L. Kuznetsov, Materials Today: Proceedings, 2017, 4, 11375-11380; https://doi.org/10.1016/j.matpr.2017.09.012

[14] S. Goswami, R. Ghosh, H. Hirani, N. Mandal, Ceram. Int., 2022, 48, 11879-11908; https://doi.org/10.1016/j.ceramint.2022.02.214

[15] W. A. Shah, X. Luo, B. I. Rabiu, B. Huang, Y. Q. Yang, Chemical Physics Letters, 2021, 781, 138978; https://doi.org/10.1016/j.cplett.2021.138978

[16] T. Mustafa, J. L. Huang, J. Gao, P. Yan, Y. P. Liu, K. H. Ruiz, S. K. Sun, J. S. Du, Y. C. Fan, W. Jiang, J. Eur. Ceram. Soc., 2021, 41, 5541-5547; https://doi.org/10.1016/j.jeurceramsoc.2021.05.004

[17] Z. Cheng, N. Andy, A. Arvind, Nanomaterials and Energy, 2016, 5, 1-9.

[18] M. Estili, A. Kawasaki, H. Sakamoto, Y. Mekuchi, M. Kuno, T. Tsukada, Acta Mater., 2008, 56, 4070-4079; https://doi.org/10.1016/j.actamat.2008.04.029

[19] T. Mustafa, Y. Liu, J. Gao, P. Yan, Q. Ding, Y. Fan, W. Jiang, Journal of Materiomics, 2023, 9, 993-1003; https://doi.org/10.1016/j.jmat.2023.03.005

[20] I. Palaci, S. Fedrigo, H. Brune, C. Klinke, M. Chen, E. Riedo, Phys. Rev. Lett., 2005, 94, 4; https://doi.org/10.1103/PhysRevLett.94.175502

[21] T. Mustafa, M. M. A. Aslam, K. H. Ruiz, M. Javed, J. Gao, M. H. Sharif, S. Khan, Ceram. Int., 2023, 49, 40478-40485; https://doi.org/10.1016/j.ceramint.2023.10.024

[22] W. M. Zeng, N. Y. Chen, Q. Y. Chen, Trans. Nonferrous Met. Soc. China, 1997, 7, 132-134.

[23] B. Lee, M. Y. Koo, S. H. Jin, K. T. Kim, S. H. Hong, Carbon, 2014, 78, 212-219; https://doi.org/10.1016/j.carbon.2014.06.074

[24] S. Sarkar, P. K. Das, Ceramics International, 2014, 40, 7449-7458; https://doi.org/10.1016/j.ceramint.2013.12.092

[25] B. Yazdani, Y. Xia, I. Ahmad, Y. Zhu, J. Eur. Ceram. Soc., 2015, 35, 179-186; https://doi.org/10.1016/j.jeurceramsoc.2014.08.043

[26] U. A. Khan, A. Hussain, M. Shah, M. Shuaib, F. Qayyum, in 14th International Symposium on Advanced Materials, eds. S. Qaisar, A. N. Khan, E. A. Mukhtar, Iop Publishing Ltd, Bristol, 2016, vol. 146; https://doi.org/10.1088/1757-899X/146/1/011001

[27] M. Hrubovčáková, E. Múdra, R. Bureš, A. Kovalčíková, R. Sedlák, V. Girman, P. Hvizdoš, J. Eur. Ceram. Soc., 2020, 40, 4818-4824; https://doi.org/10.1016/j.jeurceramsoc.2020.03.072

[28] Y. Fan, M. Estili, G. Igarashi, W. Jiang, A. Kawasaki, J. Eur. Ceram. Soc., 2014, 34, 443-451; https://doi.org/10.1016/j.jeurceramsoc.2013.08.035

[29] L. Esquivias, P. Rivero-Antúnez, C. Zamora-Ledezma, A. Domínguez-Rodríguez, V. Morales-Flórez, J. Sol-Gel Sci. Technol., 2019, 90, 162-171; https://doi.org/10.1007/s10971-018-4834-4

[30] C. Gun, X. Luo, W. A. Shah, J. K. Li, B. Huang, M. A. Umer, Y. Q. Yang, Ceram. Int., 2020, 46, 17449-17460; https://doi.org/10.1016/j.ceramint.2020.04.039

[31] E. J. Hearn, in Mechanics of Materials 2 (Third Edition), ed. E. J. Hearn, Butterworth-Heinemann, Oxford, 1997, DOI: https://doi.org/10.1016/B978-075063266-9/50011-1, pp. 381-442; https://doi.org/10.1016/B978-075063266-9/50011-1

[32] B. Chen, S. Li, H. Imai, J. Umeda, M. Takahashi, K. Kondoh, Micron, 2015, 69, 1-5; https://doi.org/10.1016/j.micron.2014.10.005

[33] B. Chen, L. Jia, S. Li, H. Imai, M. Takahashi, K. Kondoh, Advanced Engineering Materials, 2014, 16, 972-975; https://doi.org/10.1002/adem.201400232

[34] J. Luo, R. Stevens, J. Eur. Ceram. Soc., 1997, 17, 1565-1572; https://doi.org/10.1016/S0955-2219(97)00014-9

[35] Y. Chen, K. Balani, A. Agarwal, Scripta Materialia, 2012, 66, 347-350; https://doi.org/10.1016/j.scriptamat.2011.11.026

[36] X. S. Zhang, L. W. Yang, H. T. Liu, M. Zu, Rsc Adv, 2017, 7, 23334-23341;

https://doi.org/10.1039/C7RA03339G
[37] W. D. Shen, B. Jiang, B. S. Han, S. S. Xie, Phys. Rev. Lett., 2000, 84, 3634-3637; https://doi.org/10.1103/PhysRevLett.84.3634
[38] M. Estili, Y. Sakka, Sci. Technol. Adv. Mater., 2014, 15, 25; https://doi.org/10.1088/1468-6996/15/6/064902
[39] P. M. Ajayan, T. W. Ebbesen, Rep. Prog. Phys., 1997, 60, 1025-1062; https://doi.org/10.1088/0034-4885/60/10/001
[40] M. Estili, A. Kawasaki, Y. Pittini-Yamada, I. Utke, J. Michler, Journal of Materials Chemistry, 2011, 21, 4272-4278; https://doi.org/10.1039/c0jm03906c